

Evaluation of Dibenzocyclooctyne and Bicyclononyne Click Reaction on Azido-Functionalized Antifouling Polymer Brushes via Microspotting

Bingquan Yang, Yangxin Wang, Mariia Vorobii, Eric Sauter, Meike Koenig, Ravi Kumar, Cesar Rodriguez-Emmenegger, and Michael Hirtz*

Strain-promoted alkyne-azide cycloaddition (SPAAC) has become an indispensable tool in bioorthogonal conjugation and surface immobilization. While numerous studies have focused on enhancing the reactivity of cyclooctynes, a facile method to evaluate the binding efficiency for cyclooctyne-azide-based immobilization without any sophisticated facilities is still missing. In the present work, different derivatives of dibenzocyclooctyne/bicyclononyne (DBCO/BCN) linked to either a fluorophore or a biotin-moiety are patterned on ultra-low fouling polymer brushes, which can avoid unspecific protein contamination without any prior blocking steps. The polymer brushes are composed of an antifouling bottom block and azide-terminated top block. The assessment of binding efficiency is conducted on ordered arrays spotted by microchannel cantilever spotting (μ CS) with a normal fluorescent microscope. Both cyclooctynes demonstrate reliable binding performance with azide-bearing diblock polymer brushes via μ CS, but DBCO shows a higher surface density of molecular immobilization according to the protein binding assays. This work provides a reference for choosing appropriate cyclooctyne to couple with azides and can be useful for the design of biosensors or bio-platforms for analyte detection, cell capture, and other biological applications.

click reactions at the beginning of the 21st century,^[1] these reactions are consistently a vital link in the process of biosensing, cell screening, drug delivery, and bio-functionalization.^[2–8] The metal-free click reactions have circumvented the need for toxic catalysts (e.g., Cu^I) and offer a fast reaction rate.^[9,10] A successful example is benefitting from the activation by ring strain in the structure of reactants, for example, cycloalkyne or cycloalkane.^[11–15] Particularly, the strain-promoted alkyne-azide cycloaddition (SPAAC) is an outstanding member of this class owing to its excellent chemical stability, non-toxic and mild reaction conditions, and high coupling efficiency for bio-orthogonal conjugations.^[16–19]


Commonly, azide derivatives are used as bio-tags in biochemistry due to easy integration with biomolecules, for example, in metabolic labeling for living cells with azido functionality,^[20,21] post-synthetic modification,^[22,23] and in vitro enzymatic transfer.^[24,25] Attention has been placed on

enhancing the reactivity of cyclooctynes—being the other half in SPAAC—as part of the reactive probes in bio-conjugations. After the first recognition of the potential in the combination of cyclooctyne with bio-conjugation by Bertozzi and coworkers in 2004,^[26] click chemistry has entered a new metal-free era. Plenty of research groups have contributed by expanding the

1. Introduction

Recently, surfaces possessing both resistances to protein fouling and reactive groups to undergo covalent functionalization have drawn much attention in biological research, especially examples based on click chemistry approaches. Since the advent of

B. Yang, Y. Wang, R. Kumar, M. Hirtz
Institute of Nanotechnology (INT) & Karlsruhe Nano Micro Facility (KNMFi)
Karlsruhe Institute of Technology (KIT)
76344 Eggenstein-Leopoldshafen, Germany
E-mail: michael.hirtz@kit.edu

 The ORCID identification number(s) for the author(s) of this article can be found under <https://doi.org/10.1002/admi.202102325>.

© 2022 The Authors. Advanced Materials Interfaces published by Wiley-VCH GmbH. This is an open access article under the terms of the Creative Commons Attribution License, which permits use, distribution and reproduction in any medium, provided the original work is properly cited.

DOI: 10.1002/admi.202102325

M. Vorobii, C. Rodriguez-Emmenegger
DWI – Leibniz Institute for Interactive Materials and
Institute of Technical and Macromolecular Chemistry
RWTH Aachen University
52074 Aachen, Germany

E. Sauter, M. Koenig
Institute of Functional Interfaces (IFG)
Karlsruhe Institute of Technology (KIT)
76344 Eggenstein-Leopoldshafen, Germany

C. Rodriguez-Emmenegger
Institute for Bioengineering of Catalonia (IBEC)
The Barcelona Institute of Science and Technology (BIST)
Carrer de Baldiri Reixac 10-12, Barcelona 08028, Spain

C. Rodriguez-Emmenegger
Institutació Catalana de Recerca i Estudis Avançats (ICREA)
Passeig Lluís Companys 23, Barcelona 08010, Spain

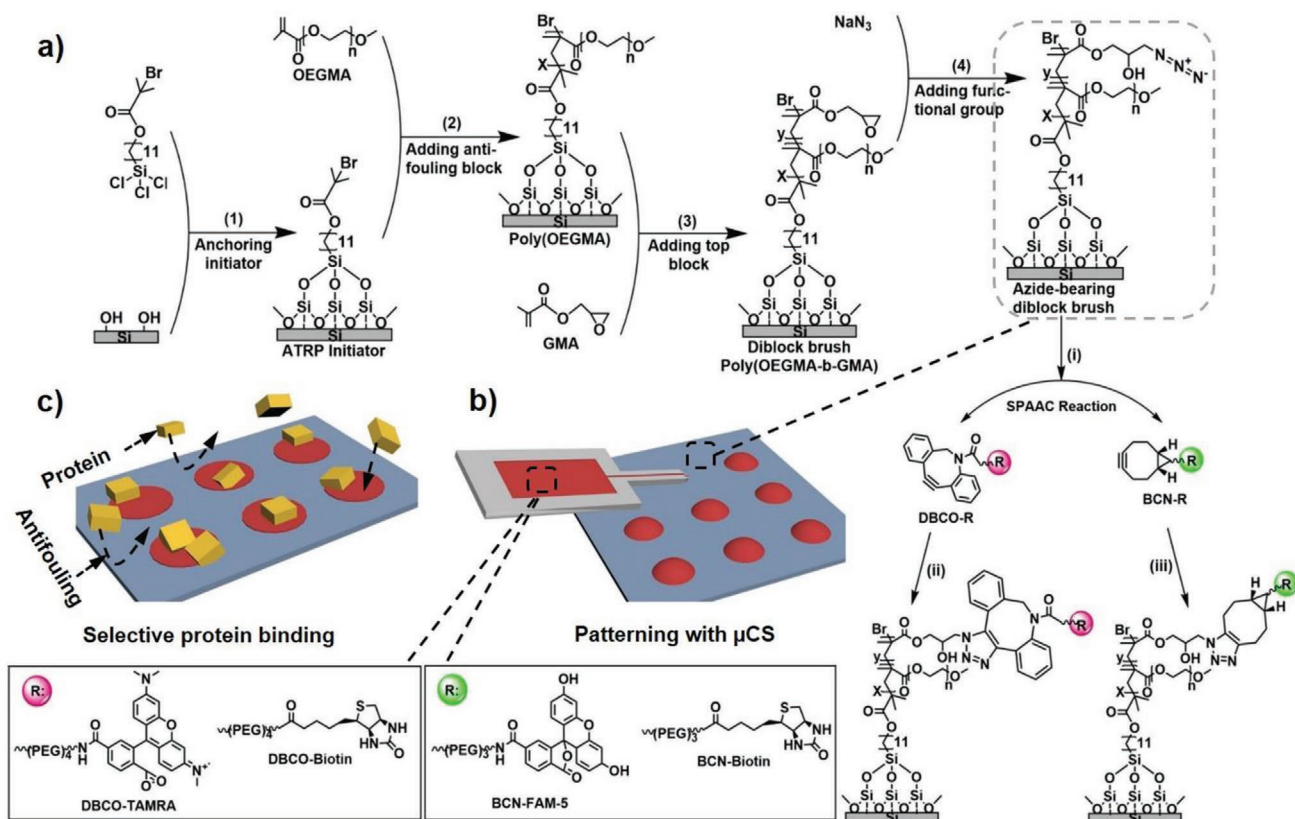


Figure 1. Schematic drawing of a) the growth process and chemical binding strategies for coupling to the azide-bearing diblock polymer brushes. b) Schemes of capturing arrays spotted by μ CS to the polymer brush surface for c) selective protein coupling. The insets show the DBCO and BCN derivatives used in the site-specific functionalization.

usage of cyclooctynes and enhancing their reactivity toward azides. This was done to enlarge the utility and improve the reactivity of SPAAC. Several cyclooctyne variants have been employed in bio-conjugations (Figure S1, Supporting Information), which can be roughly classified into aryl-containing variants and saturated systems.^[27–31] The two most commonly used representatives of each type are dibenzocyclooctyne (DBCO)^[27] and bicyclononyne (BCN),^[28] respectively.^[31] Currently available cyclooctynes were mostly developed to enhance the reactivity to azides via modulation either by fluorination,^[32,33] sp^2 -hybridization of ring atoms,^[34] or by fusion to cyclopropane.^[28] DBCO and BCN are used for SPAAC in bio-conjugations because of their relatively simple synthesis with sufficient yield and great coupling efficiency. Other cyclooctynes have comparatively low reactivity or a tedious synthetic procedure.^[27,28,35–38]

As a whole, SPAAC is an effective and crucial tool in bio-research and bio-applications, for example, in biosensors or for surface modification in biological experiments, but there is still a lack of facile and generalized ways for studying the relative coupling efficiency between cyclooctynes and azides. The aforementioned reports all rely on expensive and complex facilities to obtain the rate constant for comparison.

The use of polymer brushes to encode different functionalities alongside their structure such as stealth properties, functional groups for further functionalization, and many more which include copolymers,^[39–42] block copolymers^[43–46] and terpolymers^[47] were reported.

In 2010, the DBCO functionalized brushes for orthogonal functionalization of the surface with azide containing molecules were presented.^[48] They developed azide-containing antifouling polymer brushes that can be functionalized using DBCO-conjugated biomolecules while not impairing the antifouling properties.^[49] This served to facilitate detection of target proteins in blood plasma. Here, DBCO or BCN derivatives acted as bio-receptors. Recently, another report^[50] proved that the site-specific immobilization of cyclooctynes on azide-modified polymer brushes via printing of microarrays was possible. Utilizing lithographic approaches makes it feasible to investigate the difference in binding efficiency of conjugations between DBCO/azide and BCN/azide through quantified fluorescence measurements with a fluorescence microscope using a compound linked to the same binding motif (here biotin) to be able to attach the identical type of fluorescent protein, avoiding changes in the fluorophore emission profile that could affect a fluorescent moiety directly on the DBCO or BCN molecule (Figure 1). To elucidate this approach and quantify the different reactivity, we synthesized antifouling polymer brushes bearing azide-modified terminal groups as the lithography substrate, and then immobilized various DBCO and BCN derivatives via microchannel cantilever spotting (μ CS). To obtain a high number of functional groups, side chain functionalization was implemented on copolymer building block brushes.^[51] Additionally, to minimize side effects due to the thickness of the top block on antifouling properties, the thickness of the top

Table 1. Contact angle, thickness, and roughness reports of the films of the surfaces. Every mean value with standard deviation was computed from 3 measurements at random positions.

Surface state	Water contact angle [°]		Thickness ^{a)} [nm]	Roughness ^{a)} [nm]
	Advancing	Receding		
Glass (before hydroxylation)	49.2 ± 2.6	31.6 ± 2.7	–	0.155 ± 0.017
Glass (after hydroxylation)	– ^{b)}	– ^{b)}	–	–
SAM initiator	87.2 ± 2.8	58.6 ± 2.3	1.8 ± 0.2	0.124 ± 0.013
Poly(OEGMA)	55.5 ± 1.5	34.3 ± 1.8	24.3 ± 0.5	0.372 ± 0.030
Poly(OEGMA-b-GMA)	53.1 ± 2.9	34.2 ± 1.7	32.7 ± 0.6	0.532 ± 0.093
Azide functionalized poly(OEGMA-b-GMA)	85.0 ± 3.1	46.4 ± 2.6	31.5 ± 0.4	0.503 ± 0.086

^{a)}Si wafer modified with polymer brushes was used for thickness and roughness (mean roughness, R_a) measurements in dry conditions with ellipsometer and AFM, respectively; ^{b)}The contact angle was too low to be determined due to higher hydrophilicity after treatment with plasma cleaning.

layer was adjusted to ≈ 8 nm, following our previous work.^[49] Generally, the polymer brush consists of two building blocks: the bottom block is an inert layer, highly-protein repelling and therefore does not require any blocking steps in the performed specific protein binding studies; the top block is a reactive layer functionalized with azide groups, which can participate in the SPAAC reaction. Based on these properties, a protein binding assay was implemented to obtain an accurate and quantitative comparison of immobilization efficiency, as well as confirming the feasibility of intended applications for these polymer brushes in microarray-based biosensing for the two SPAAC regimes.

2. Results and Discussions

Interfaces combining reactive and antifouling properties, possessing adjustable reactive sites, and remarkable capabilities of protein repellency are playing a significant role in constructing platforms for label-free biosensing, biological research, and other applications.^[41,52–54] Polymer brushes, especially those with hierarchical architectures, are a remarkable candidate to meet the aforementioned needs. Generally, the excellent self-cleaning performance benefiting from the densely packed non-fouling molecules and the adjustable reactive groups at the polymer chain end can provide customizable terminals for satisfying diverse demands. Typically, azides are a widely used substance to introduce such activated sites for binding biomolecules or analytes based on SPAAC reactions. In the present work, the azide-bearing diblock polymer brushes were utilized to repel protein and react with strained alkynes.

Patterning molecular arrays on substrates with μ CS is strongly impacted by surface properties, therefore wettability and roughness of the surface in each state of growing the polymer brush were investigated and the successful chemical functionalization was monitored. For this, the dynamic water contact angle (WCA) measurements, ellipsometry, atomic force microscopy (AFM), and X-ray photoelectron spectroscopy (XPS) were conducted. WCA testing is a facile and effective way to study the altering of the surface wettability induced by changes in the chemical surface state. On this ground, the dynamic WCA was performed for the substrates in each

modification step and the corresponding results are shown in **Table 1**. Initially, the formation of a self-assembled monolayer (SAM) of the silane ATRP-initiator on a freshly oxygen plasma-treated substrate leads to a sudden rise in WCA from 0 to 87° as well as is identified clearly by the C 1s XP spectrum (details below in XPS section). For inspection of the SAM quality, thickness and morphology measurements were conducted with ellipsometry and AFM, respectively, on silicon substrates prepared in parallel with the glass specimens. As shown in Table 1 the thickness is 1.8 nm, and the corresponding AFM image (**Figure 2a**) exhibits the uniform and smooth topography of the surface. All in all, the results above demonstrate successful SAM formation. With reference to the SAM, the WCA on the surface with the bottom block [poly(OEGMA)] including both, the advancing and receding angle, drops sharply, as expected

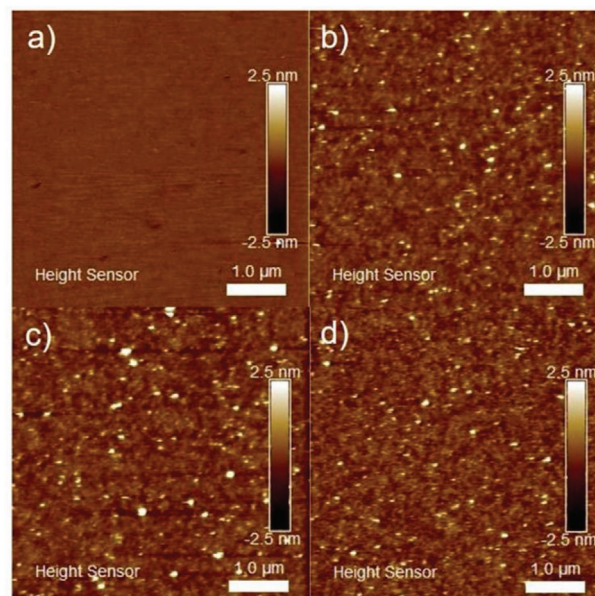


Figure 2. Surface topography of specimens at various stages within the polymer brush growth process imaged by AFM. a) ATRP initiator, b) poly(OEGMA), c) poly(OEGMA-b-GMA), d) azide-bearing poly(OEGMA-b-GMA). Corresponding roughnesses are given in Table 1. All scale bars equal 1 μ m.

by the introduction of the hydrophilic polymer side chains. Typically, the decline of the receding WCA is greater compared with the advancing WCA owing to the strong interaction of the swollen polymer layers with water.^[44] Similar phenomena of wettability occurred on the copolymer surface [poly(OEGMA-*b*-GMA)]. On introduction of the azide groups to the polymer brush, the dynamic WCA converted back to a higher value, indicating that the functionalization was successful. The moderate hydrophilicity of the completed substrate offers a stable interface to adhere ink dots spotted by μ CS (where very low WCA would make the printed spots spread and merge together with adjacent ones, finally destroying the orientated pattern arrays).

In parallel with the inspection of the dynamic WCA, measurements of surface topography were implemented to survey the variation in roughness, further corroborating the development of polymer brushes. Generally, μ CS works best on smooth interfaces, as large roughness may cause difficulties for ink transfer and for constructing ordered dot arrays. Figure 2 shows AFM images of surfaces at the different stages during the process of polymer brush growing. As can be seen, after grafting of ATRP initiator the surface morphology barely changes compared to bare silicon (Figure S3, Supporting Information), the surface morphology remains smooth and the mean roughness (R_a) is (0.124 ± 0.013) nm.

The synthesis of the first layer of the bilayer polymer brushes induced a significant increase in roughness (R_a , from (0.124 ± 0.013) nm to (0.372 ± 0.030) nm), caused by the generation of sequential and well-oriented compact structures of poly(OEGMA) on the SAM initiator surface, indicating that the antifouling block was successfully grafted. Similarly again, a further increase in roughness (R_a , from (0.372 ± 0.030) nm to (0.532 ± 0.093) nm) suggests the successful chain extension with GMA and formation of poly(OEGMA-*b*-GMA). However, the image also shows that the overall homogeneous and rather smooth interface was maintained even as the former step changed roughness. In the last preparation step, after azido functionalization of the terminal groups, the roughness stays constant (R_a , from (0.532 ± 0.093) nm to (0.503 ± 0.086) nm), which is also expected as of the small size of the added azido

group, thus the terminal change in brush structure is not much varying the surface morphology.

XPS was employed to thoroughly characterize and identify the chemical compositions of the diblock polymer brushes, and the results are illustrated in Figure 3. First, the silane initiator formed a SAM of 1.8 nm on a freshly treated substrate. As plotted in Figure 3a-1, a strong peak appears at 285.0 eV and is attributed to C–C and C–H in the scaffold of the alkane of the initiator. Additionally, the C–O and O=C–C within the ester group induce two relatively weak peaks at 286.8 and 289.0 eV, respectively. The scale distribution of the three peaks originating from the initiator is consistent with its chemical structure where the bonds C–C and C–H occupy the major quotient in the structure, but only one ester group exists. The acquired XPS data of the antifouling block is shown in Figure 3a-2. The addition of macromolecular [poly(OEGMA)] adds mass of C–O all along the side chains of the polymer and raises the proportion of C–O within the structure, therefore leading to a predominant signal at 286.5 eV. In addition, the signal at 289.0 eV can be attributed to the contribution of O=C–C in the methacrylate backbone. Consequently, the area ratio between the (C–O) and (C–C, C–H) is ≈ 3.74 . Above the ≈ 22 nm layer of poly(OEGMA) a layer of poly(GMA) with ≈ 8 nm thickness was grown. Layers of the same magnitude have been shown to possess excellent properties for conjugation and protein repellence, though the relative thicknesses of each layer might deviate to some extent by blending between the two blocks.^[50] Figure 3a-3 depicts the XP spectrum of the copolymer [poly(OEGMA-*b*-GMA)] collected in C 1s region. By contribution from the grafted poly(GMA) block, the intensity of the signal of all the sorts of covalent bonds in the copolymer structure is strengthened. Accordingly, the area ratio of (C–O):(C–C, C–H) drops to 2.61. Figure 3a-4 and b-4 picture the XP spectra of azido functionalized copolymer in the C 1s and N 1s region, respectively. The epoxide groups were attacked by NaN_3 dissolved in DMF and a ring-opening reaction took place, therefore endowing azido groups to the polymer brush. As expected, there was no signal recorded in the N 1s region from copolymers [poly(OEGMA-*b*-GMA)] before functionalization with the azide. According to a previous report,^[37] high energy X-ray beams can destroy the

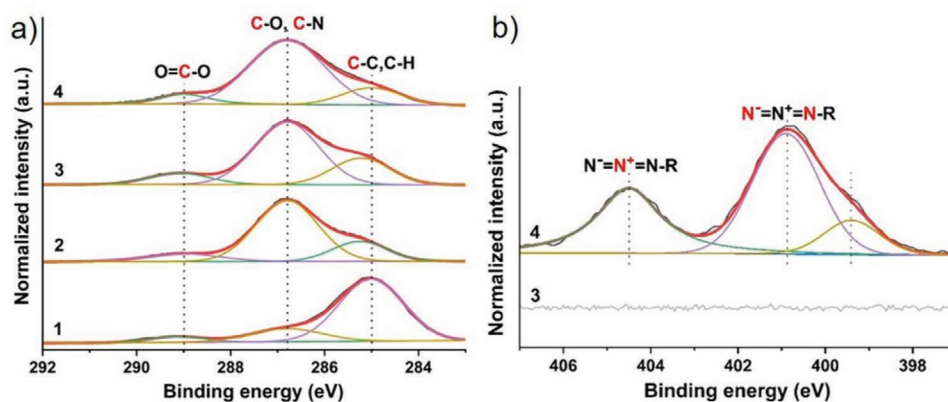


Figure 3. a) XPS characterization at C 1s region of different surfaces, 1) ATRP initiator, 2) poly(OEGMA), 3) poly(OEGMA-*b*-GMA), 4) poly(OEGMA-*b*-(3-azido-2-hydroxypropyl methacrylate)). b) XPS characterization at N 1s region of poly(OEGMA-*b*-GMA) 3) before and 4) after azide functionalization. The components resulting from corresponding chemical species are highlighted in red. All spectra are normalized to the corresponding maximum intensity.

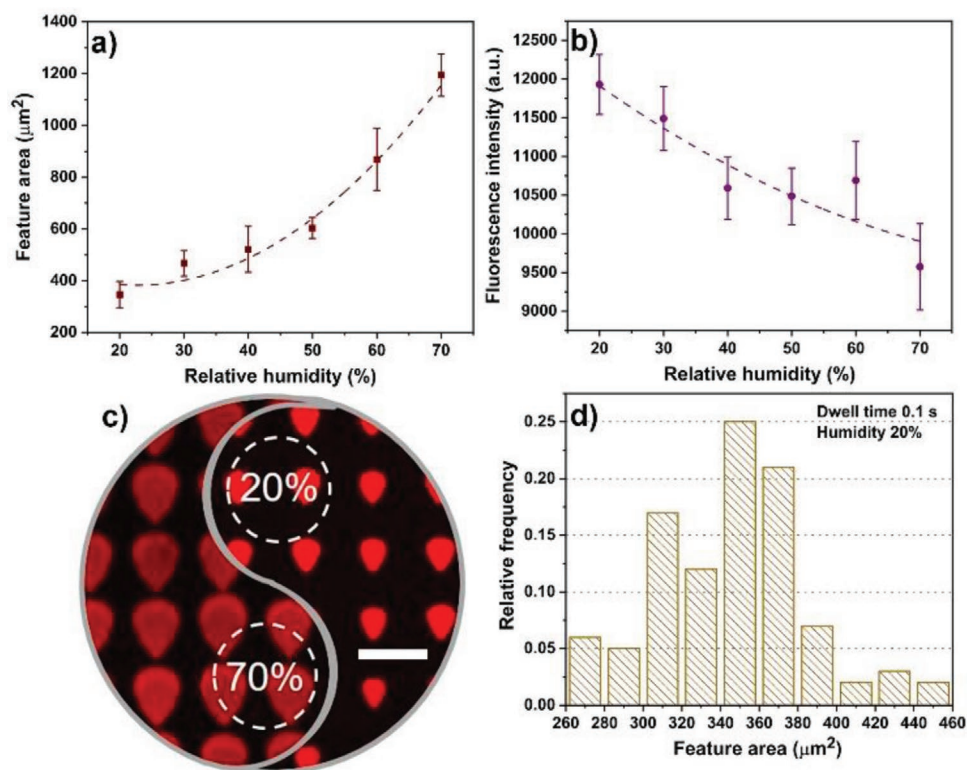


Figure 4. Dependence of a) feature size and b) relative fluorescence intensity on humidity of DBCO-Tamra on azide-bearing diblock polymer brushes; and c) fluorescent micrographs captured with exposure time 5 ms on two diverse patterns printed at dwell time of 0.1 s but at two different relative humidity situations, 20% and 70%, respectively; d) the corresponding feature area distribution of the microarray in (c) written at relative humidity of 20%. Scale bar is 50 μm .

structure of polymers and degrade the azido groups gradually, this is a plausible reason to explain the small signal that appears at 399.4 eV in Figure 3b-4. Peaks at 400.9 and 404.5 eV are accurate signal feedback of azido moieties, confirming the terminal substitution and formation of azide-bearing diblock polymer brushes.

After establishing the successful synthesis of the desired polymer brush, two types of representative cyclooctynes, aryl-containing cyclooctyne (DBCO) and saturated system (BCN), were employed to explore the difference of the immobilization density and efficiency on azide-bearing brushes between the two cyclooctynes. In order to establish the optimum lithography regime for the target inks in μCS , microarrays including 100 dots were patterned into 10×10 matrices with a pitch of 50 μm at different printing parameters. On the fully functionalized polymer brushes, fluorescent arrays remained visible even after washing away excess ink, while (as negative control) arrays printed on substrates of bare glass and diblock polymer brushes without azide poly(OEGMA-*b*-GMA) vanish after washing (Figure S6, Supporting Information).

Humidity as a major factor in printing was studied initially, since it highly controls the speed of the ink transfer and can alter the concentration of the spotted ink by drying or hygroscopic action. Figure 4 pictures the feature size and relative fluorescence intensity on polymer brushes of DBCO-TAMRA ink written at a humidity range from 20% to 70%. As illustrated in Figures 4a,b, the feature size (as here denoted by feature

area) has a positive correlation with increasing humidity, but negative for fluorescence intensity. A possible explanation here is that the ink solution collects extra water vapor from the humidity in the atmosphere, which lowers ink viscosity and concentration, hence leading to faster ink flow and giving a bigger size yet weaker fluorescence intensity of spots. In addition, raised environmental humidity will also affect the polymer brush hydration and thus lower the contact angle of the deposited droplet, further increasing the feature size and area over which the ink volume is spread. Typical images captured on specimens printed at 20% and 70% relative humidity are shown in Figure 4c and the corresponding feature size distribution on a 20% sample is given in Figure 4d.

Dwell time (tip/sample contact time during feature spotting) is another crucial parameter to govern the feature dimension and its size distribution. Figure 5 shows the results of DBCO-TAMRA by tuning the dwell time. Evidently, the dwell time only affects the feature dimension, but not fluorescence intensity, as the amount of deposited ink contains much more molecules for immobilization than binding sites are available at the footprint of the droplet feature, thus overall deposited volume does not affect the amount of bound compound per area. Results of the same set of experiments with BCN-FAM ink following similar trends are given in the Supporting Information (Figures S4 and S5, Supporting Information). Based on these results and to obtain a narrow feature size distribution and highest fluorescence intensity, we fixed printing parameters for DBCO and

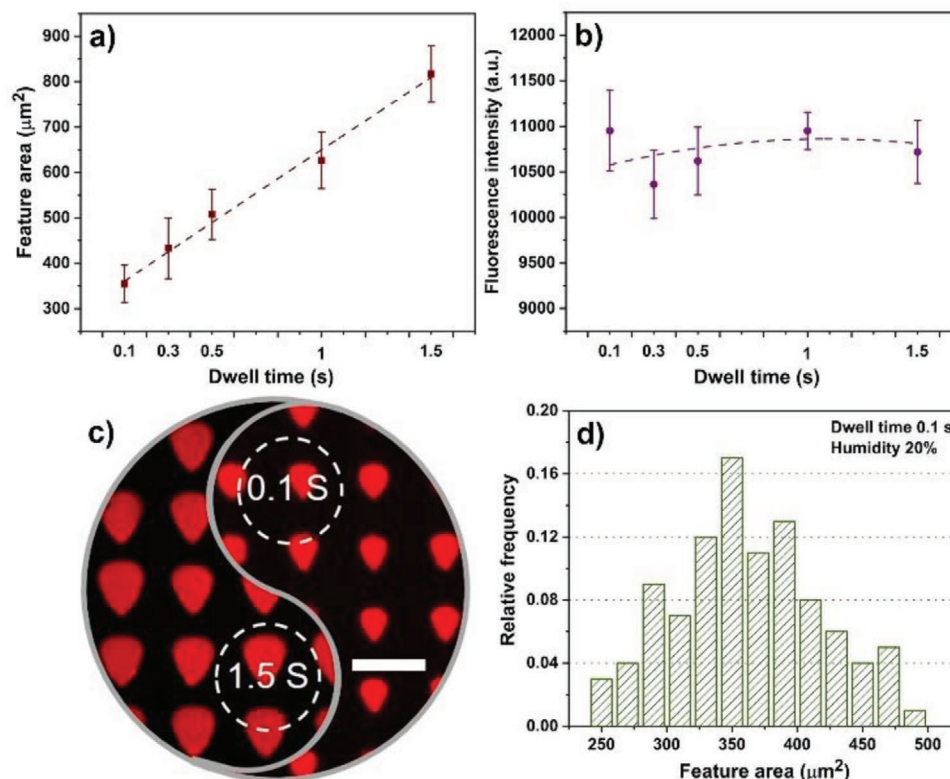


Figure 5. Dependence of a) feature dimension and b) relative fluorescence intensity on dwell time of DBCO-Tamra on azide-bearing diblock polymer brushes. c) Fluorescent images taken on two microarrays printed at relative humidity of 20% but dwell time of 0.1 and 1.5 s, with exposure time 5 ms. d) The corresponding feature dimension distribution of micropattern in (c) written at dwell time 0.1 s. Scale bar is 50 μm .

BCN derivatives for the remaining experiments to a humidity of 20% (both) and dwell time of 0.1 s and 0.5 s, respectively.

Reaction time and temperature are two vital factors in click reactions. Therefore, to evaluate the efficiency of SPAAC reaction between azide and cyclooctynes in μCS , the printed samples were allowed to rest for various reaction durations at room temperature (25 $^{\circ}\text{C}$) and at slightly elevated “physiological” temperature (37 $^{\circ}\text{C}$) for comparison. The results for fluorophore-DBCO conjugate ink immobilized on the azide-bearing diblock brushes (10×10 matrices with a pitch of 50 μm , optimal DBCO conditions for humidity and dwell time of 20% r.H., 0.1 s) are shown in **Figure 6**. Here, the observed fluorescence intensity can be seen as a measure of the amount of coupled molecules.

The fluorescence intensity increases with reaction time for 15 min thereafter reaching saturation for both at 25 and 37 $^{\circ}\text{C}$. Moreover, an elevated temperature (37 $^{\circ}\text{C}$) speeds up the reaction, thus the fluorescence reaches the plateau already after 15 min incubation at 37 $^{\circ}\text{C}$, but only after 20 min at 25 $^{\circ}\text{C}$. Beyond these time points, the obtained intensity shows only slight fluctuation which means that there is no more coupling going on and the binding attains saturation. Figures 6c and d exhibit the series of fluorescent images corresponding to the intensity graph in Figures 6a,b. All in all, we conclude that the optimal reaction condition for azide/DBCO in the probed parameter space is 15 min at 37 $^{\circ}\text{C}$, attaining the highest fluorescence intensity but consuming the lowest time.

The same approach (printing of 10×10 matrices with a pitch of 50 μm , optimal conditions for BCN of 20% r.H.,

0.5 s dwell time) was then repeated to assess the reaction situation of azide/BCN. After finishing of spotting, the samples were allowed to incubate for a series of reaction times at 25 and

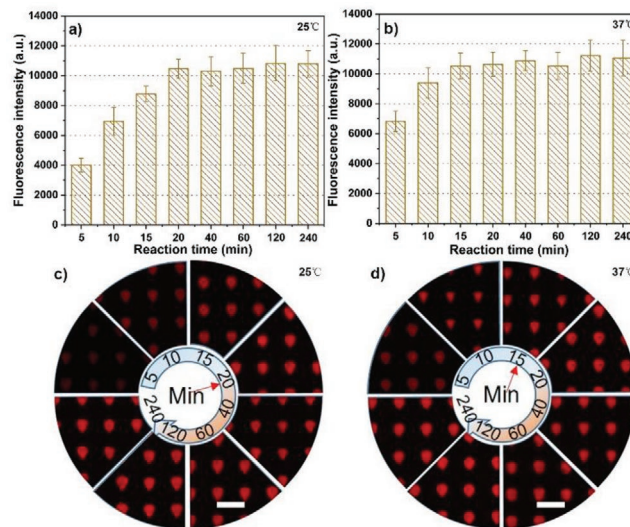


Figure 6. Relationship of the relative fluorescence intensity with the reaction time and temperature of the DBCO-Tamra microarrays on azide-bearing diblock polymer brushes, a) at room temperature, b) at 37 $^{\circ}\text{C}$; c) and d) are the corresponding fluorescent images to (a) and (b), respectively. Exposure time for images are 5 ms, scale bars are 50 μm .

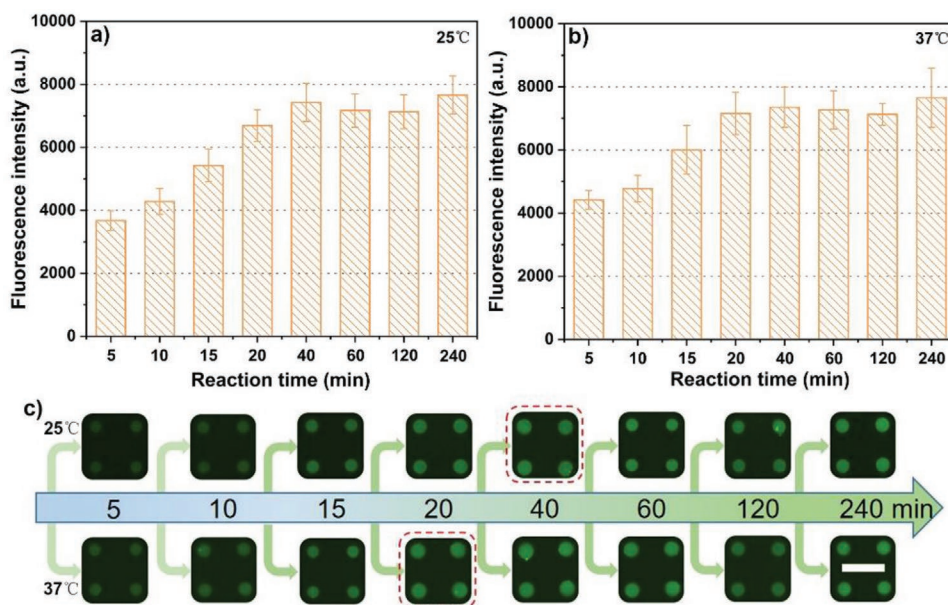


Figure 7. Relationship of the relative fluorescent intensity with the reaction time and temperature of the BCN-FAM micropatterns on azide functionalized hierarchical polymer brushes a) at room temperature, b) at 37 °C; c) the corresponding fluorescent images to (a) and (b), respectively. Exposure time for images are 100 ms, scale bar is 50 μm .

37 °C, respectively. The corresponding results are illustrated in **Figure 7**. The optimum reaction time for azide/BCN at both 25 and 37 °C was prolonged to 40 and 20 min, respectively. This is in accordance to the respective behavior in bulk labeling where such a delay possibly can be ascribed to the benzofusion in DBCO enhancing the reaction rate compared to BCN. The corresponding fluorescence microscopy images can be found in **Figure 7c**. Accordingly, the reaction time of 20 min at 37 °C was deemed as optimal within the probed printing parameters for azide/BCN and is selected for further experiments in the present work.

As the emission of fluorescent compounds will usually differ with modifications of the molecule, it is not straightforward to compare DBCO and BCN derivatives directly (and in our case, we chose different fluorophores (TAMRA and FAM) with different spectra altogether). To enable a direct comparison of binding efficiency regarding immobilization density, we probed non-fluorescent derivatives that enable binding of

the fluorophore-labeled protein (streptavidin-Cy3) over biotin-streptavidin binding, so that both derivatives can be probed with the same fluorophore. Avidin and especially streptavidin has been widely used in immunoassays and other biological research and analysis due to binding biotin with high affinity and specificity.^[55,56]

To accomplish the comparison aforementioned, two types of biotin inks, DBCO-PEG₄-Biotin and BCN-PEG₃-Biotin, were spotted on the azide-bearing diblock polymer brushes with a series concentrations from 500 to 3000 $\mu\text{g mL}^{-1}$ in 10×10 matrices with a pitch of 50 μm . Before implementing the incubation step with streptavidin-Cy3, the samples were allowed to rest at 37 °C for 15 and 20 min, respectively, for the coupling of DBCO-Biotin and BCN-Biotin. The chart in **Figure 8a** gives the comparison of fluorescent intensity collected from the immobilized microarrays after binding with Cy3-conjugated streptavidin, and corresponding fluorescent images are shown in **Figure 8b** and **c**, respectively. The selective binding

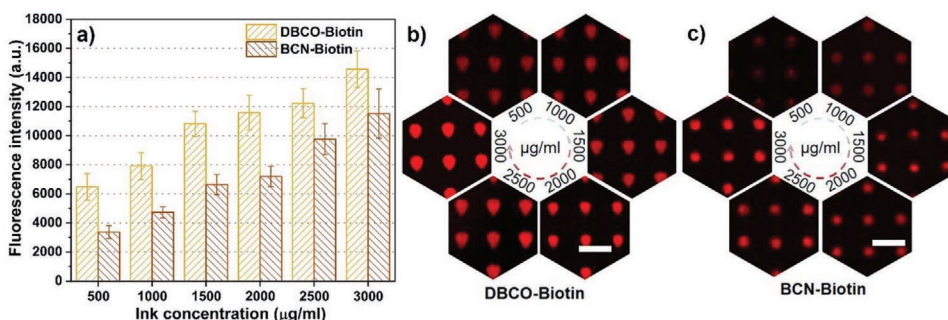


Figure 8. Influence of ink concentration on relative fluorescence intensity of a) biotin (linked with DBCO or BCN) immobilized on azide-bearing diblock polymer brushes after incubating with STV-Cy3 (resting time at 37 °C after printing, 15 min for DBCO-Biotin, 20 min for BCN-Biotin). Printing settings for DBCO-Biotin of humidity was 20% and dwell time was 0.1 s, for BCN-Biotin was 20% and 0.5 s, respectively. (b) and (c) are the corresponding fluorescent images after incubation of STV-Cy3 for DBCO-Biotin and BCN-Biotin, respectively. Exposure time is 50 ms, Scale bars equal 50 μm .

of the fluorescently labeled protein to the array features already acts as an intrinsic control for the antifouling properties of the azide-bearing brush (i.e., the areas in between the array features remain dark in fluorescence). Additionally, we conducted dedicated antifouling studies and demonstrated that functionalization of poly(OEGMA) brushes with azide-bearing diblock and further immobilization of biotin do not affect their resistance to unspecific protein adsorption (Figure S7, Supporting Information). The fluorescence intensity gathered on DBCO-Biotin patterns is stronger than the one gathered on BCN-Biotin patterns in each ink concentration column. In detail, the fluorescence intensity varies from (6487.24 ± 912.93) to $(14\,567.92 \pm 1263.81)$ for DBCO-Biotin and from (3368.22 ± 438.24) to $(11\,510.79 \pm 1698.74)$ for BCN-Biotin following the increase of ink concentration.

The data shows that the fluorescence intensity at the same ink concentration of the DBCO modified sample is ≈ 1.3 – 1.9 -fold higher than on the BCN modified ones. This is particularly interesting because the ink of the same weight concentration contains $\approx 26\%$ more molecules of BCN-Biotin (594.31 g mol^{-1}) in comparison to DBCO-PEG₄-Biotin (749.92 g mol^{-1}). Based on obtained data, we can conclude that in μCS the binding of azide/DBCO is more efficient than the binding of azide/BCN.

3. Conclusion

The presented work described a systematic investigation of the coupling efficiency of small molecules delivered via μCS to azide functionalized diblock polymer brushes. Two representative cyclooctynes (DBCO and BCN) in fluorescent modifications and biotin derivatives were utilized in creating micropatterns by immobilization at azide groups through SPAAC reaction at different temperatures, reaction times, and concentrations. The results show that higher temperature promoted the process of the click reactions and gave optimized reaction conditions for azide/DBCO and azide/BCN at 15 min ($37\text{ }^\circ\text{C}$) and 20 min ($37\text{ }^\circ\text{C}$), respectively. Importantly, by direct comparison of the streptavidin-Cy3 fluorescence coupled to the polymer brush via biotin-DBCO and biotin-BCN, we found that the binding efficiency of the azide/DBCO coupling was significantly higher (≈ 1.3 – 1.9 -fold) for azide/BCN at the two reaction regimes. Therefore, our conclusions suggest using DBCO derivatives to bind with azides to attain higher surface density of the immobilized target molecules. Our results can act as reference for choice of biorthogonal reagents in surface immobilization and offer important information for the fabrication of click-chemistry based microarrays.

4. Experimental Section

Materials: All chemicals used in the present study were used as received and without any purification procedures. [11-(2-Bromo-2-Methyl) Propionyloxy] Undecyltrichlorosilane (ATRP-initiator) was provided by Cymit (Spain). CuBr, CuBr₂, NaN₃, 2,2'-bipyridyl, oligo (ethylene glycol) methyl ether methacrylate ($M_n = 300\text{ g mol}^{-1}$, OEGMA) and glycidyl methacrylate (GMA) were purchased from Sigma-Aldrich (Germany). Dibenzylcyclooctyne-PEG₄-5/6-tetramethylrhodamine (DBCO-Tamra) and dibenzylcyclooctyne-PEG₄-biotin conjugate (DBCO-Biotin) were

obtained from Jena Bioscience (Germany). 5-carboxyfluorescein-PEG₃-BCN (BCN-FAM) and biotin-PEG₃-BCN (BCN-Biotin) were purchased from Conju-Probe (USA). N,N-dimethylformamide (DMF), dichloromethane, chloroform, methanol, ethanol, acetone, phosphate-buffered saline (PBS), streptavidin-Cy3, and toluene were purchased from Sigma-Aldrich (Germany). Aluminum oxide 90 basic was purchased from Carl Roth (Germany). Ultrapure water was produced in lab by an Arium Pro system from Sartorius (Germany).

Substrate Pre-Treatment and Grafting of Initiator: Before doing plasma cleaning, substrates (either silicon wafer ($10 \times 10\text{ mm}$, used in AFM and ellipsometry characterizations) or round glass substrates (13 mm diameter, for fluorescence microscopy)) were sonicated in chloroform, ethanol, and water for 5 min each, and then dried with a stream of nitrogen. After this, substrates were plasma treated (10 sccm O_2 , 0.2 mbar , and 100 W) in an ATTO system, Diener electronics (Germany) for 20 min. Without delay, the hydroxylated substrates were soaked in a freshly prepared solution of initiator in anhydrous toluene (1 mg mL^{-1}) for 3 h. To obtain a homogeneously SAM initiator on the glass surface, the grafting procedure was done in a dry environment. When finished, the substrates were rinsed with toluene, acetone, ethanol, and water and then blown with nitrogen for drying before the next step.

Grafting of the Diblock Polymer Brushes: The polymer brushes employed in the present work possessed a diblock hierarchical structure. The bottom layer of the diblock polymer brushes was an antifouling layer and responsible for the antifouling property, the top layer was a reactive layer modified with azide groups. The full synthesis protocol can be found in the literature.^[57,58] The inhibitors were removed by passing the monomers through an alumina column. Here the protocol is depicted concisely: As the whole reaction process must be in oxygen-free conditions, all the containers and mixtures were deoxygenized with N₂ for 1 h before implementing the next steps. For synthesis of the bottom layer, methanol (5 mL), catalysts, and monomer solution were placed in three round-bottom flasks and degassed with N₂ for 1 h, separately. The catalyst mixture contained 2,2'-bipyridyl (155 mg, 991 μmol), CuBr₂ (16.8 mg, 75 μmol), and CuBr (53.8 mg, 375 μmol). A solution of OEGMA (5.9 g, 19 mmol) in 5 mL ultrapure water constituted the monomer solution. After 1 h of degassing, methanol (5 mL) was transferred into the flask containing catalysts and then stirred under N₂ protection to obtain the catalyst solution. Without delay, the monomer solution was transferred into the flask containing the catalyst solution to obtain the precursor solution. Subsequently, the precursor solution was gently injected into a container containing the initiator SAM-modified substrates under N₂ environment. The reaction was conducted at $30\text{ }^\circ\text{C}$ for 30 min, and then stopped by removing the substrates from the container. The substrates were rinsed with ethanol and water twice and dried with a stream of nitrogen. The ellipsometric thickness of obtained poly(OEGMA) layer was $\approx 24.3\text{ nm}$ in dry condition.

The next two procedures were growing the top layer of the polymer brushes and functionalizing the epoxy terminals with azido groups. Here, the poly(OEGMA) obtained in the last step acted as macroinitiators for growing of the top block. Fresh GMA without inhibitor (6.7 mL, 49 mmol), dry N,N-Dimethylformamide (DMF, 10 mL), 2,2'-bipyridyl (191 mg, 1222 μmol), and CuBr₂ (21.8 mg, 98 μmol) were added to a round-bottom flask and bubbled with N₂ for 1 h, after which CuBr (70.1 mg, 489 μmol) was added, and then the mixture was stirred thoroughly until full dissolution. Straight after, the fully mixed solution was slowly injected into a previously deoxygenated reactor containing the poly(OEGMA) coated substrates obtained in the last step. The growth was allowed to proceed at $60\text{ }^\circ\text{C}$ for 6 h. Subsequently, the substrates were removed from the reactor and rinsed with DMF, dichloromethane, acetone, and water twice of each and dried under a stream of nitrogen. The entire dry thickness of the poly(OEGMA-b-GMA) was 32.7 nm, and the corresponding thickness of the top block, therefore, 8.4 nm. To finally obtain the azido functionalized diblock polymer brushes, a nucleophilic epoxide ring-opening with azide was carried out by immersing the substrates into a solution of NaN₃ (3.4 mg mL^{-1}) in anhydrous DMF at $60\text{ }^\circ\text{C}$ for 24 h. Afterward, the substrates were rinsed with DMF, ethanol, and water twice of each and dried with nitrogen.

Ink Solution Preparation: In order to prevent premature evaporation of the inks during printing, all solutions were admixed with glycerol. For storage, inks were kept in dark at $-20\text{ }^{\circ}\text{C}$. The concentration of the fluorescent dyes employed (DBCO-Tamra and BCN-FAM) in a mixture of DMSO/glycerol (7:3, v/v) was $500\text{ }\mu\text{g mL}^{-1}$. Analogously, DBCO-Biotin and BCN-Biotin, were dissolved at a concentration range from 500 to $3000\text{ }\mu\text{g mL}^{-1}$ in a mixture of DMSO/glycerol (7:3, v/v).

Patterning Process with μCS : The detailed spotting strategy for surface patterns can be found in other reports,^[59] briefly described: prior to mounting the quill-like pen called surface patterning tool (SPT) probes (SPT-S-C30S, Bioforce Nanosciences, USA) on a holder, probes were hydroxylated by oxygen plasma activation (10 sccm O_2 , 0.2 mbar, 100 W, for 2 min, ATTO plasma system, Diener electronics, Germany). After activation, $0.2\text{ }\mu\text{L}$ of ink solution was loaded on the reservoir of the probe immediately and then it was mounted to the holder on a NLP 2000 system (NanoInk, USA) to conduct pattern writing. Dot patterns were designed of 10×10 spot arrays with a pitch of $50\text{ }\mu\text{m}$ in each direction. Typically, the spotting procedures were implemented at a series of relative humidity in the range of $\approx 20\text{--}70\%$ and various dwell times from $\approx 0.1\text{--}1.5\text{ s}$.

Coupling of Dot Arrays: After surface patterning, the target molecules, DBCO-Tamra and BCN-FAM, were allowed to couple to the diblock polymer brush coated substrates for different durations in the range of 5 to 240 min at either $25\text{ or }37\text{ }^{\circ}\text{C}$, respectively. Subsequently, samples were rinsed with PBS 3 times to remove excess ink and then blew dry with nitrogen. A similar protocol was performed for the non-fluorescent targets (Biotin-DBCO/BCN) with different concentrations at a fixed temperature of $37\text{ }^{\circ}\text{C}$ for 15 min/20 min, respectively.

Protein Binding on Biotinylated Dot Arrays: A fluorescently labeled protein, streptavidin-Cy3, was used to bind with the immobilized biotin derivatives. In this procedure, the merits of diblock polymer brushes were exhibited thoroughly. Usually, bovine serum albumin (BSA) or a similar agent was necessary as a blocking reagent for the protein binding process, but in the present work, the antifouling block of the diblock polymer brushes conveniently allowed to omit the blocking process completely. The arrayed biotin derivatives were incubated with $100\text{ }\mu\text{L}$ of 1 mg mL^{-1} streptavidin-Cy3 in PBS (1:100) at $37\text{ }^{\circ}\text{C}$ for 30 min in a dark environment. Subsequently, samples were rinsed with PBS 3 times and blown dry under a stream of nitrogen before fluorescence microscopy.

Sample Characterization: The thickness of the polymer brushes was measured by spectroscopic ellipsometry (M 2000, Woollam Co., Inc., Lincoln NE, USA) on silicon substrates in dry conditions at an incident angle of 65° in the wavelength range of $\lambda = 370\text{--}900\text{ nm}$. All measurements were evaluated with an optical box model on the software CompleteEase, and silicon substrates were all fitted with standard values for Si and SiO_2 as defined in the software. The thickness and the optical properties of the polymer layers were fitted with a Cauchy relation model. The dynamic WCA measurements were performed on an OCA-20 contact angle analyzer (DataPhysics Instruments GmbH, Germany) at room temperature. Briefly, this was done by placing a water droplet of $20\text{ }\mu\text{L}$ on the substrate, then the volume was increased up to $50\text{ }\mu\text{L}$ at a rate of $0.5\text{ }\mu\text{L s}^{-1}$, followed by decreasing the volume again at the same rate. The whole process was conducted automated by the onboard software and recorded by the built-in camera. Finally, the advancing and receding contact angles were obtained by fitting the drop profile with the circular fitting algorithm of the instruments onboard software. To evaluate the changing surface roughness of substrates during the growing process of the polymer brushes, an AFM (Dimension Icon, Bruker, Germany) was employed. All measurements were conducted at room temperature in the air in contact mode (Cantilever type was ScanAsyst-Air, 0.4 N m^{-1} , Bruker, Germany). For each sample, 3 random positions were scanned (each $5 \times 5\text{ }\mu\text{m}^2$) and the roughness R_a extracted by the onboard software of the instrument. The fluorescent images were recorded on a Nikon Eclipse 80i upright fluorescence microscope (Nikon, Japan) integrated with an Intensilight illumination (Nikon, Japan), a CoolSNAP HQ2 camera (Photometrics, USA), and Texas Red and FITC filters (Nikon Y-2E/C). The ^1H nuclear magnetic resonance (NMR) spectrum of

the initiator (Figure S2, Supporting Information) was recorded in Chloroform-d on a Bruker Avance 500 spectrometer at $25\text{ }^{\circ}\text{C}$. The ^1H NMR chemical shifts (δ) were given in ppm and referred to the residual protons on the deuterated solvent. The XPS measurements were carried out under ultra-high vacuum conditions with a base pressure of 1×10^{-9} mbar. Core-level spectra were recorded under normal emission with a Scienta R4000 hemispherical electron analyzer using Al-K_{α} radiation (1486.6 eV). First, for every sample the survey XP spectrum was measured and no unexpected contaminations were observed in these spectra. Then, the detailed Si 2p, C 1s, N 1s, O 1s XP spectra were recorded. For a precise determination of the C 1s and N 1s lines position and necessary correction the XPS Peak 41 software was used. All spectra were fitted with Voigt profile (20% of Lorentz-Gaussian contribution) using linear background for XY peak and Shirley background for YZ peak. The line correction was adjusted to C 1s peak at 285.0 eV .

Supporting Information

Supporting Information is available from the Wiley Online Library or from the author.

Acknowledgements

This work was carried out with the support of the Karlsruhe Nano Micro Facility (KNMFi, www.knmf.kit.edu), a Helmholtz Research Infrastructure at Karlsruhe Institute of Technology (KIT, www.kit.edu). B.Y. acknowledges support by the China Scholarship Council fellowship (No. 201807040067, CSC, www.csc.edu.cn).

Open access funding enabled and organized by Projekt DEAL.

Conflict of Interest

The authors declare no conflict of interest.

Data Availability Statement

The data that support the findings of this study are available from the corresponding author upon reasonable request.

Keywords

coupling efficiency, microchannel cantilever spotting, strain-promoted alkyne-azide cycloaddition, ultra-low fouling hierarchical polymer brushes

Received: November 26, 2021

Revised: February 28, 2022

Published online:

- [1] M. G. F. Hartmuth, C. Kolb, K. Barry Sharpless, *Angew. Chem., Int. Ed.* **2001**, *40*, 2004.
- [2] L. Liang, D. Astruc, *Coord. Chem. Rev.* **2011**, *255*, 2933.
- [3] R. Kumar, A. Bonicelli, S. Sekula-Neuner, A. C. B. Cato, M. Hirtz, H. Fuchs, *Small* **2016**, *12*, 5330.
- [4] Y. Chen, Y. Xianyu, J. Wu, B. Yin, X. Jiang, *Theranostics* **2016**, *6*, 969.
- [5] Y. Liu, M. Liu, Y. Zhang, Y. Cao, R. Pei, *New J. Chem.* **2020**, *44*, 11420.
- [6] S. M. M. Dadfar, S. Sekula-Neuner, V. Trouillet, M. Hirtz, *Adv. Mater. Interfaces* **2021**, *8*, 2002117.

- [7] P. Destito, C. Vidal, F. Lopez, J. L. Mascarenas, *Chem. - Eur. J.* **2021**, *27*, 4789.
- [8] O. Guselnikova, J. Váňa, L. T. Phuong, I. Panov, L. Rulišek, A. Trelin, P. Postnikov, V. Švorčík, E. Andris, O. Lyutakov, *Chem. Sci.* **2021**, *12*, 5591.
- [9] S. Li, G. Li, B. Gao, S. P. Pujari, X. Chen, H. Kim, F. Zhou, L. M. Klivansky, Y. Liu, H. Driss, D. D. Liang, J. Lu, P. Wu, H. Zuilhof, J. Moses, K. B. Sharpless, *Nat. Chem.* **2021**, *13*, 858.
- [10] P. Jonkheijm, D. Weinrich, H. Schroder, C. M. Niemeyer, H. Waldmann, *Angew. Chem., Int. Ed.* **2008**, *47*, 9618.
- [11] E. M. Sletten, C. R. Bertozzi, *Acc. Chem. Res.* **2011**, *44*, 666.
- [12] P. M. E. Gramlich, C. T. Wirges, A. Manetto, T. Carell, *Angew. Chem., Int. Ed.* **2008**, *47*, 8350.
- [13] B. Albada, J. F. Keijzer, H. Zuilhof, F. van Delft, *Chem. Rev.* **2021**, *121*, 7032.
- [14] D. Gahtory, R. Sen, A. R. Kuzmyn, J. Escorihuela, H. Zuilhof, *Angew. Chem., Int. Ed.* **2018**, *57*, 10118.
- [15] J. Escorihuela, W. J. E. Looijen, X. Wang, A. J. A. Aquino, H. Lischka, H. Zuilhof, *J. Org. Chem.* **2020**, *85*, 13557.
- [16] M. P. S. Chang-Fang Wang, E. Mäkilä, M. L. K. Hyvönen, P. M. Laakkonen, J. J. Salonen, J. T. Hirvonen, A. J. Airaksinen, H. A. Santos, *Biomaterials* **2015**, *48*, 108.
- [17] G. Xu, P. Liu, D. Pranantyo, K.-G. Neoh, E.-T. Kang, S. Lay, -M. Teo, *ACS Sustainable Chem. Eng.* **2019**, *7*, 1786.
- [18] L. G. L. E. Murrell, *ACS Comb. Sci.* **2020**, *22*, 109.
- [19] J. T. Ling Chu, J. E. Shaw, F. Rivera-Molina, A. J. Koleske, A. Schepartz, D. K. Toomre, *Nat. Commun.* **2020**, *11*, 4271.
- [20] J. M. Baskin, C. R. Bertozzi, *QSAR Comb. Sci.* **2007**, *26*, 1211.
- [21] E. Zhang, Y. Shi, J. Han, S. Han, *Anal. Chem.* **2020**, *92*, 15059.
- [22] E. M. Sletten, C. R. Bertozzi, *Angew. Chem., Int. Ed.* **2009**, *48*, 6974.
- [23] B. Josephson, C. Fehl, P. G. Isenegger, S. Nadal, T. H. Wright, A. W. J. Poh, E. J. Bower, A. M. Giltrap, L. Chen, C. Batchelor-McAuley, G. Roper, O. Arisa, J. B. I. Sap, A. Kawamura, A. J. Baldwin, S. Mohammed, R. G. Compton, V. Gouverneur, B. G. Davis, *Nature* **2020**, *585*, 530.
- [24] M. Fernandez-Suarez, H. Baruah, L. Martinez-Hernandez, K. T. Xie, J. M. Baskin, C. R. Bertozzi, A. Y. Ting, *Nat. Biotechnol.* **2007**, *25*, 1483.
- [25] Y. Zhang, K.-Y. Park, K. F. Suazo, M. D. Distefano, *Chem. Soc. Rev.* **2018**, *47*, 9106.
- [26] J. A. P. Nicholas, J. Agard, R. Bertozzi, *J. Am. Chem. Soc.* **2004**, *126*, 15046.
- [27] M. F. Debets, S. S. van Berkel, S. Schoffelen, F. P. Rutjes, J. C. van Hest, F. L. van Delft, *Chem. Commun.* **2010**, *46*, 97.
- [28] J. Dommerholt, S. Schmidt, R. Temming, L. J. Hendriks, F. P. Rutjes, J. C. van Hest, D. J. Lefeber, P. Friedl, F. L. van Delft, *Angew. Chem., Int. Ed.* **2010**, *49*, 9422.
- [29] C. R. B. Ellen, M. Sletten, *Org. Lett.* **2008**, *10*, 3097.
- [30] Z. Geng, J. J. Shin, Y. Xi, C. J. Hawker, *J. Polym. Sci.* **2021**, *59*, 963.
- [31] M. F. Debets, S. S. van Berkel, Jan Dommerholt, A. (Ton) J. Dirks, Floris P. J. T. Rutjes, Floris L. van Delft, *Acc. Chem. Res.* **2011**, *44*, 805.
- [32] J. M. Baskin, J. A. Prescher, S. T. Laughlin, N. J. Agard, P. V. Chang, I. A. Miller, A. Lo, J. A. Codelli, C. R. Bertozzi, *Proc. Natl. Acad. Sci. USA* **2007**, *104*, 16793.
- [33] J. M. B. Julian, A. Codelli, N. J. Agard, C. R. Bertozzi, *J. Am. Chem. Soc.* **2008**, *130*, 11486.
- [34] A. P. Alexander Kuzmin, M. A. Wolfert, V. V. Popok, *Bioconjugate Chem.* **2010**, *21*, 2076.
- [35] J. M. B. Nicholas, J. Agard, J. A. Prescher, A. Lo, C. R. Bertozzi, *ACS Chem. Biol.* **2006**, *1*, 644.
- [36] X. Ning, J. Guo, M. A. Wolfert, G.-J. Boons, *Angew. Chem., Int. Ed.* **2008**, *120*, 2285.
- [37] E. M. S. John, C. Jewett, C. R. Bertozzi, *J. Am. Chem. Soc.* **2010**, *132*, 3688.
- [38] C. G. Gordon, J. L. Mackey, J. C. Jewett, E. M. Sletten, K. N. Houk, C. R. Bertozzi, *J. Am. Chem. Soc.* **2012**, *134*, 9199.
- [39] H. Vaisocherova-Lisalova, F. Surman, I. Visova, M. Vala, T. Springer, M. L. Ermini, H. Sipova, P. Sedivak, M. Houska, T. Riedel, O. Pop-Georgievski, E. Brynda, J. Homola, *Anal. Chem.* **2016**, *88*, 10533.
- [40] H. Lisalova, E. Brynda, M. Houska, I. Visova, K. Mrkvova, X. C. Song, E. Gedeonova, F. Surman, T. Riedel, O. Pop-Georgievski, J. Homola, *Anal. Chem.* **2017**, *89*, 3524.
- [41] T. Riedel, F. Surman, S. Hageneder, O. Pop-Georgievski, C. Noehammer, M. Hofner, E. Brynda, C. Rodriguez-Emmenegger, J. Dostálek, *Biosens. Bioelectron.* **2016**, *85*, 272.
- [42] C. Rodriguez-Emmenegger, F. Surman, E. Brynda, T. Riedel, M. Houska, H. Lisalova, J. Homola, *WO2016177354*, **2016**.
- [43] C. Rodriguez Emmenegger, E. Brynda, T. Riedel, Z. Sedlakova, M. Houska, A. B. Alles, *Langmuir* **2009**, *25*, 6328.
- [44] A. de los Santos Pereira, T. Riedel, E. Brynda, C. Rodriguez-Emmenegger, *Sens. Actuators, B* **2014**, *202*, 1313.
- [45] A. de los Santos Pereira, N. Yu. Kostina, M. Bruns, C. Rodriguez-Emmenegger, C. Barner-Kowollik, *Langmuir* **2015**, *31*, 5899.
- [46] C. J. Huang, N. D. Brault, Y. Li, Q. Yu, S. Jiang, *Adv. Mater.* **2012**, *24*, 1834.
- [47] M. Forinova, A. Pilipenco, I. Visova, N. S. Lynn, Jr., J. Dostalek, H. Maskova, V. Honig, M. Palus, M. Selinger, P. Kocova, F. Dycka, J. Sterba, M. Houska, M. Vrabцова, P. Horak, J. Anthi, C. P. Tung, C. M. Yu, C. Y. Chen, Y. C. Huang, P. H. Tsai, S. Y. Lin, H. J. Hsu, A. S. Yang, A. Dejneka, H. Vaisocherova-Lisalova, *ACS Appl. Mater. Interfaces* **2021**, *13*, 60612.
- [48] A. A. P. Sara, V. Orski, S. Arumugam, L. Mao, V. V. Popik, J. Locklin, *J. Am. Chem. Soc.* **2010**, *132*, 11024.
- [49] V. Parrillo, A. de los Santos Pereira, T. Riedel, C. Rodriguez-Emmenegger, *Anal. Chim. Acta* **2017**, *971*, 78.
- [50] U. Bog, A. de los Santos Pereira, S. L. Mueller, S. Havenridge, V. Parrillo, M. Bruns, A. E. Holmes, C. Rodriguez-Emmenegger, H. Fuchs, M. Hirtz, *ACS Appl. Mater. Interfaces* **2017**, *9*, 12109.
- [51] A. R. Kuzmyn, L. W. Teunissen, P. Fritz, B. van Lagen, M. M. J. Smulders, H. Zuilhof, *Adv. Mater. Interfaces* **2022**, *9*, 2101784.
- [52] Z. Wang, L. Scheres, H. Xia, H. Zuilhof, *Adv. Funct. Mater.* **2020**, *30*, 1908098.
- [53] C. Rodriguez-Emmenegger, S. Janel, A. de los Santos Pereira, M. Bruns, F. Lafont, *Polym. Chem.* **2015**, *6*, 5740.
- [54] I. Banerjee, R. C. Pangule, R. S. Kane, *Adv. Mater.* **2011**, *23*, 690.
- [55] J. Zempleni, S. S. Wijeratne, Y. I. Hassan, *BioFactors* **2009**, *35*, 36.
- [56] V. Balan, G. Dodi, C. T. Mihai, A. M. Serban, V. C. Ursachi, *Int. J. Biol. Macromol.* **2021**, *188*, 82.
- [57] H. Vaisocherová-Lísalová, I. Víšová, M. L. Ermini, T. Špringer, X. C. Song, J. Mrázek, J. Lamačová, N. S. Lynn Jr., P. Šedivák, J. Homola, *Biosens. Bioelectron.* **2016**, *80*, 84.
- [58] J. Striebel, M. Vorobii, R. Kumar, H.-Y. Liu, B. Yang, C. Weishaupt, C. Rodriguez-Emmenegger, H. Fuchs, M. Hirtz, K. Riehemann, *Adv. Nanobiomed. Res.* **2020**, *1*, 2000029.
- [59] C. Zhong, C. Hu, R. Kumar, V. Trouillet, F. Biedermann, M. Hirtz, *ACS Appl. Nano Mater.* **2021**, *4*, 4676.